



# Synthesis of CuO/Zn<sub>2</sub>SnO<sub>4</sub> Nanocomposites via Hydrothermal Method and Their Photocatalytic Performance for Ciprofloxacin Degradation

Rika Agustin<sup>1</sup>, Vivi Sisca<sup>2</sup>, Asdim<sup>1</sup>, Eka Angasa<sup>1,\*</sup>



<sup>1</sup> Department of Chemistry, Faculty of Mathematics and Natural Sciences, Bengkulu University, Bengkulu, Indonesia

<sup>2</sup> Research Center for Chemical, Research Organization for Nanotechnology and Materials, National Research and Innovation Agency (BRIN), Puspiptek, Serpong-South Tangerang, Indonesia

\* Corresponding author: [eka.angasa@gmail.com](mailto:eka.angasa@gmail.com)

<https://doi.org/10.14710/jksa.28.2.98-105>

## Article Info

### Article history:

Received: 15<sup>th</sup> December 2024

Revised: 21<sup>st</sup> February 2025

Accepted: 27<sup>th</sup> February 2025

Online: 28<sup>th</sup> February 2025

### Keywords:

Ciprofloxacin; CuO;  
 CuO/Zn<sub>2</sub>SnO<sub>4</sub> Nanocomposite;  
 Zn<sub>2</sub>SnO<sub>4</sub>

## Abstract

CuO/Zn<sub>2</sub>SnO<sub>4</sub> nanocomposites were successfully synthesized via a hydrothermal method at 180°C for 5 hours. The CuO/Zn<sub>2</sub>SnO<sub>4</sub> nanocomposites were developed to evaluate their potential as photocatalysts for the degradation of ciprofloxacin, a pharmaceutical pollutant commonly found in water sources. The materials were characterized using XRD, SEM, TEM, and UV-Vis DRS analyses. XRD results confirmed that the CuO/Zn<sub>2</sub>SnO<sub>4</sub> nanocomposites, prepared with various CuO concentrations (20, 40, 60, and 80% w/w), exhibited good crystallinity and high purity. SEM analysis revealed that the morphology of the composites consisted of square-shaped nanosheets resembling CuO and irregular, round particles with non-uniform sizes resembling Zn<sub>2</sub>SnO<sub>4</sub>. TEM analysis further confirmed that the CuO/Zn<sub>2</sub>SnO<sub>4</sub> nanocomposite with 40% CuO exhibited irregular square and round nanosheets with an average size of 69.53 nm. UV-Vis DRS analysis showed that the band gap of pure Zn<sub>2</sub>SnO<sub>4</sub> (3.22 eV) decreased after the incorporation of CuO, with values of 1.67 eV (20%), 1.46 eV (40%), 1.50 eV (60%), and 1.50 eV (80%). The photocatalytic activity of the nanocomposites was evaluated based on the degradation of ciprofloxacin under sunlight irradiation. The degradation percentages of pure Zn<sub>2</sub>SnO<sub>4</sub>, pure CuO, and CuO/Zn<sub>2</sub>SnO<sub>4</sub> with 20% CuO were 78.3%, 8.9%, and 47.1%, respectively. This study demonstrates that the CuO/Zn<sub>2</sub>SnO<sub>4</sub> nanocomposite has fewer active surface sites than pure Zn<sub>2</sub>SnO<sub>4</sub>, which significantly influences its photocatalytic performance.

## 1. Introduction

Along with technological advancements and increasing energy demands, environmental pollution has become a global and pressing issue that continues to attract the attention of researchers seeking effective solutions. One of the industries contributing significantly to environmental pollution is the pharmaceutical industry, which generates toxic and hazardous waste both during production and post-consumption, including antibiotic waste [1]. In recent years, numerous studies have reported a substantial increase in antibiotic concentrations in rivers, lakes, groundwater, and even drinking water [2]. In addition to deteriorating water quality, the presence of these antibiotics promotes the

emergence of drug-resistant bacteria, thereby reducing the effectiveness of antibiotics and posing long-term risks to human health [3].

Among the various treatment methods developed, the photocatalytic method using semiconductor materials has been recognized as one of the most effective approaches for degrading ciprofloxacin waste [4]. Ternary metal oxides have emerged as promising semiconductor alternatives to binary oxides, offering several advantages, such as higher corrosion resistance, greater structural stability, tunable physicochemical properties, and a wider selection of material compositions [5, 6]. Examples of ternary metal oxides

include  $\text{ZnBi}_2\text{O}_4$  [7],  $\text{ZnFe}_2\text{O}_4$  [8],  $\text{CuAl}_2\text{O}_4$  [9], and  $\text{CuFe}_2\text{O}_4$  [10].

One of the ternary metal oxides that have attracted significant attention from researchers is zinc stannate ( $\text{Zn}_2\text{SnO}_4$ ), owing to its excellent semiconductor properties. These include stability under extreme conditions, low cost, non-toxicity, a wide band gap energy (3.6 eV), high electron mobility ( $112 \text{ cm}^2\text{V}^{-1}\text{s}^{-1}$ ), and high electrical conductivity ( $10^4 \text{ S cm}^{-1}$ ) [5, 11, 12, 13, 14]. Currently,  $\text{Zn}_2\text{SnO}_4$  has been widely applied in various fields, such as photocatalysis, solar cells, and sensors [15, 16, 17, 18]. However, its wide band gap limits its applicability to UV irradiation, thereby restricting its practical use. Additionally, the large band gap can lead to rapid recombination of electron ( $e^-$ ) and hole ( $h^+$ ) pairs, which reduces its quantum efficiency and photocatalytic performance [19].

Therefore, it is necessary to modify  $\text{Zn}_2\text{SnO}_4$  to reduce its band gap and inhibit the rapid recombination of charge carriers. One strategy that has been developed is coupling  $\text{Zn}_2\text{SnO}_4$  with other semiconductors that possess narrower band gaps, thereby extending its light absorption into the visible region [20]. Several studies have reported the successful coupling of  $\text{Zn}_2\text{SnO}_4$  with other semiconductors to reduce its band gap, including  $\text{Zn}_2\text{SnO}_4/\text{V}_2\text{O}_5$  [21],  $\text{BiVO}_4/\text{Zn}_2\text{SnO}_4$  [22], and  $\text{BiOBr}/\text{Zn}_2\text{SnO}_4$  [20].

In this study,  $\text{Zn}_2\text{SnO}_4$  was modified by compositing it with  $\text{CuO}$  at various concentrations through a hydrothermal process.  $\text{CuO}$  is a *p*-type semiconductor with a narrow band gap energy (1.4–1.75 eV), is non-toxic, abundantly available, has a high penetration coefficient, and exhibits good photocatalytic activity [17, 23, 24]. The phase structure, morphology, and band gap values of the resulting  $\text{CuO}/\text{Zn}_2\text{SnO}_4$  nanocomposites were characterized using X-ray diffraction (XRD), scanning electron microscopy (SEM), transmission electron microscopy (TEM), and ultraviolet-visible diffuse reflectance spectroscopy (UV-Vis DRS).

The photocatalytic performance of the nanocomposites in degrading the antibiotic ciprofloxacin was evaluated under direct sunlight irradiation, with the reduction in ciprofloxacin absorbance measured using a UV-Vis spectrophotometer. The synthesized  $\text{CuO}/\text{Zn}_2\text{SnO}_4$  nanocomposites exhibited good crystallinity and high purity, with irregular square and round nanosheets measuring approximately 69.53 nm.

In addition, the nanocomposites demonstrated enhanced light absorption in the visible region, as indicated by a reduction in band gap values from 3.22 eV (pure  $\text{Zn}_2\text{SnO}_4$ ) to 1.46, 1.50, and 1.67 eV. This study shows that the presence of  $\text{CuO}$  in  $\text{Zn}_2\text{SnO}_4$  reduces the surface area and pore volume while increasing the pore size of the  $\text{CuO}/\text{Zn}_2\text{SnO}_4$  nanocomposites, which are the dominant factors affecting the photocatalytic performance of the resulting composites.

## 2. Experimental

### 2.1. Materials and Tools

The materials used in this study included zinc acetate dihydrate ( $\text{Zn}(\text{CH}_3\text{COO})_2 \cdot 2\text{H}_2\text{O}$ , Merck,  $\geq 99.5\%$  purity), tin(IV) chloride ( $\text{SnCl}_4$ , Sigma-Aldrich, 98% purity), copper(II) nitrate trihydrate ( $\text{Cu}(\text{NO}_3)_2 \cdot 3\text{H}_2\text{O}$ , Merck, 99.98% purity), sodium hydroxide ( $\text{NaOH}$ , Merck, pro analysis grade), demineralized water (Brataco), Hyundai filter paper No. 53, universal pH paper, and ciprofloxacin HCl 500 mg (Hexpharm Jaya).

The instruments used in this study included an XRD (PANalytical Philips), SEM (FEI Inspect-S50), TEM (JEM-1400), UV-Vis DRS (Shimadzu UV-2401-PC), UV-Vis spectrophotometer (Analytik Jena Specord 210),  $\text{N}_2$  adsorption-desorption analyzer (Micromeritics TriStar II 3020), oven (Philip Harris Ltd.), analytical balance (Sartorius), and a hydrothermal reactor.

### 2.2. Synthesis of $\text{Zn}_2\text{SnO}_4$ Using Hydrothermal Method

The synthesis of  $\text{Zn}_2\text{SnO}_4$  via the hydrothermal method was carried out following previously reported procedures [15, 18]. A 0.1 M  $\text{SnCl}_4$  solution (10 mL) and a 0.2 M  $\text{Zn}(\text{CH}_3\text{COO})_2 \cdot 2\text{H}_2\text{O}$  solution (10 mL) were mixed and stirred using a magnetic stirrer at 700 rpm for 10 minutes at room temperature. Subsequently, 20 mL of 0.4 M  $\text{NaOH}$  solution was added to the mixture and stirred for an additional 30 minutes. The resulting mixture was then transferred into a hydrothermal reactor and heated at  $185^\circ\text{C}$  for 17 hours in an oven. After completion of the reaction, the reactor was allowed to cool to room temperature. The mixture was then filtered using Hyundai No. 53 filter paper and washed with demineralized water until a neutral pH was achieved. The resulting precipitate was dried at  $85^\circ\text{C}$  for 15 hours. The obtained powder samples were then characterized using XRD, SEM, TEM, and UV-Vis DRS.

### 2.3. Synthesis of $\text{CuO}/\text{Zn}_2\text{SnO}_4$ Composite Using Hydrothermal Method

The synthesis of  $\text{CuO}/\text{Zn}_2\text{SnO}_4$  composites was carried out by modifying the procedure reported in previous studies using the hydrothermal method [25, 26, 27]. First, 40 mL of 0.0225 M  $\text{Cu}(\text{NO}_3)_2 \cdot 3\text{H}_2\text{O}$  solution was stirred at 700 rpm for 10 minutes. Then, 20 mL of 0.2 M  $\text{NaOH}$  solution was slowly added over 10 minutes while stirring. Subsequently, an appropriate amount of  $\text{Zn}_2\text{SnO}_4$  was added, corresponding to the desired  $\text{CuO}$  concentration (0, 20, 40, 60, and 80% w/w), and the mixture was stirred for an additional 10 minutes. The resulting solution was transferred to a hydrothermal reactor and heated at  $180^\circ\text{C}$  for 5 hours. After the reaction was complete, the reactor was allowed to cool to room temperature ( $20$ – $25^\circ\text{C}$ ). The mixture was filtered, washed with demineralized water until reaching a neutral pH, and dried at  $100^\circ\text{C}$  for 6 hours. The synthesized composites were subsequently characterized using XRD, SEM, TEM, and UV-Vis DRS.

## 2.4. Characterization

### 2.4.1. Characterization Using XRD

XRD is a technique that utilizes the interaction between X-rays and atoms arranged in a crystal lattice. XRD analysis provides information regarding the crystal structure and crystalline phases present in a material [28]. The resulting diffractogram from the XRD analysis is compared with data from the Inorganic Crystal Structure Database (ICSD) and presented in graphical form using Origin software. The full width at half maximum (FWHM) value of the diffraction peaks is used to calculate the crystallite size using the Debye–Scherrer equation (1).

$$D = \frac{K \lambda}{\beta \cos \theta} \quad (1)$$

Where,  $D$  is the crystallite size (nm),  $K$  is the constant (0.9),  $\lambda$  is the wavelength of the X-rays used,  $\beta$  is the FWHM of the diffraction peak,  $\theta$  is the Bragg diffraction angle.

### 2.4.2. Characterization Using UV-Vis DRS

UV-Vis DRS is an analytical technique for examining powders and solid surfaces [29]. The absorbance data obtained from UV-Vis DRS analysis is used to determine the band gap energy of the material by applying the Kubelka–Munk function. The band gap value is calculated using the Kubelka–Munk equation (2).

$$[F(R)hv]^n = A(hv - E_g) \quad (2)$$

Where,  $F(R)$  is the Kubelka–Munk function,  $h$  is Planck's constant,  $\nu$  is photon frequency,  $h\nu$  is photon energy,  $A$  is a constant,  $E_g$  is the optical band gap, and  $n$  is an exponent that depends on the type of electronic transition. The value of  $n$  is typically set to 1/2 for direct allowed transitions and 2 for indirect allowed transitions.

### 2.4.3. Characterization Using SEM and TEM

SEM and TEM were conducted to determine the morphology of  $Zn_2SnO_4$ , CuO, and CuO/ $Zn_2SnO_4$  composite samples. SEM typically produces images of the sample surface and elemental mapping images to show the sample's composition. The images obtained from SEM are black and white, as the probe electrons used are outside the visible light spectrum [30]. SEM characterization of  $Zn_2SnO_4$  samples was performed at magnifications of 100,000 $\times$  and 150,000 $\times$ . Meanwhile, TEM uses electrons as the light source, which have much shorter wavelengths, allowing for a resolution up to 1,000 times greater than a conventional light microscope.

### 2.4.4. Photodegradation of Ciprofloxacin HCl

A total of 25 mL of 20 ppm ciprofloxacin solution was mixed with 0.01 g of the CuO/ $Zn_2SnO_4$  composite. The mixture was stirred for 30 minutes using a magnetic stirrer in a dark room to achieve adsorption-desorption equilibrium. Afterward, the absorbance of the solution was measured and recorded as the initial concentration of ciprofloxacin. The mixture was then exposed to direct sunlight. The degradation process was monitored every 30 minutes between 11:00 and 14:00 WIB by taking 5 mL

aliquots of the mixture, centrifuging them, and measuring the absorbance in the wavelength range of 200–800 nm.

Subsequently, the percentage of degradation and the degradation rate of the CuO/ $Zn_2SnO_4$  composite in degrading ciprofloxacin HCl were calculated. For comparison, the same procedure was also applied under several conditions, namely without using the CuO/ $Zn_2SnO_4$  composite but exposed to sunlight, using the CuO/ $Zn_2SnO_4$  composite without irradiation (in a dark room), using  $Zn_2SnO_4$  exposed to sunlight, and using  $Zn_2SnO_4$  without irradiation (in a dark room). The data obtained from the UV-Vis spectrophotometer showed changes in the absorbance values of ciprofloxacin before and after the degradation process, and the concentrations were calculated using a standard curve. The degradation efficiency of the sample was determined by calculating the percentage of degradation using Equation (3).

$$\%P = \frac{C_0 - C_t}{C_0} \times 100\% \quad (3)$$

Where,  $P$  is the percentage of ciprofloxacin degradation,  $C_0$  is the initial concentration of the solution (ppm), and  $C_t$  is the concentration of the solution at time  $t$ .

## 3. Results and Discussion

### 3.1. XRD Analysis

The phase and structure of the synthesized products were analyzed using XRD, as presented in Figure 1. The XRD pattern shown in Figure 1a reveals sharp diffraction peaks at  $2\theta$  angles of 17.92°, 29.31°, 34.50°, 36.09°, 41.88°, 45.93°, 51.90°, 55.29°, 60.62°, 63.78°, 68.64°, 71.63°, 72.59°, 76.42°, 83.79°, and 86.47°. These peaks correspond to cubic  $Zn_2SnO_4$  with plane indices of (111), (220), (311), (222), (400), (331), (422), (511), (440), (531), (620), (533), (622), (444), (642), and (731), according to ICSD No. 024234. In addition, sharp peaks were observed at  $2\theta$  angles of 32.61°, 35.64°, 38.85°, 46.39°, 48.75°, 53.66°, 58.44°, 61.58°, 66.32°, 68.17°, 72.54°, 75.30°, 80.28°, 82.61°, 83.47°, 86.74°, and 89.95°, which are identified as monoclinic CuO with plane indices of (110), (002), (111), (-112), (-202), (020), (202), (-113), (022), (220), (311), (004), (-204), (-313), and (222), in accordance with ICSD No. 069094. These results confirm the successful synthesis of the CuO/ $Zn_2SnO_4$  composite.

The sharp and intense peaks observed for all composite samples indicate high crystallinity. A high degree of crystallinity is beneficial for photocatalysts, as it reduces the recombination rate of electron-hole pairs and provides a larger surface area for substrate adsorption, both of which significantly enhance the photocatalytic performance of the composite [31, 32]. Furthermore, the absence of additional peaks in the diffractogram suggests that the synthesized composites exhibit high purity. As shown in Figure 1b, the intensity of the CuO peaks gradually increases with the addition of higher CuO concentrations, further confirming the successful formation of CuO/ $Zn_2SnO_4$  composites with varying CuO contents.

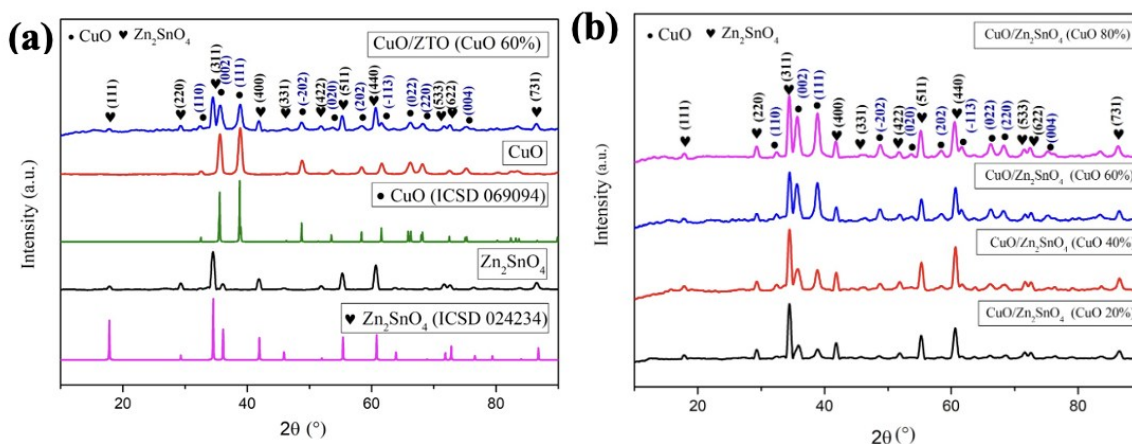


**Figure 1.** XRD diffraction patterns of the synthesized samples: (a) Zn<sub>2</sub>SnO<sub>4</sub>, CuO, and CuO/Zn<sub>2</sub>SnO<sub>4</sub> composites; (b) CuO/Zn<sub>2</sub>SnO<sub>4</sub> composites with varying CuO concentrations of 20, 40, 60, and 80% (w/w)

**Table 1.** Average crystallite size of Zn<sub>2</sub>SnO<sub>4</sub>, CuO, and CuO/Zn<sub>2</sub>SnO<sub>4</sub> composite materials

Product	Average crystal size (D) (nm)
Zn <sub>2</sub> SnO <sub>4</sub>	28.54
CuO	25.99
CuO/Zn <sub>2</sub> SnO <sub>4</sub> (CuO 20%)	29.48
CuO/Zn <sub>2</sub> SnO <sub>4</sub> (CuO 40%)	20.23
CuO/Zn <sub>2</sub> SnO <sub>4</sub> (CuO 60%)	31.99
CuO/Zn <sub>2</sub> SnO <sub>4</sub> (CuO 80%)	34.82

The average crystallite size of the synthesized products was calculated using the Debye-Scherrer equation based on the three most intense peaks for each sample. For Zn<sub>2</sub>SnO<sub>4</sub>, calculations were performed at the diffraction peaks corresponding to 2θ values of 34.50°, 51.90°, and 60.62°. For CuO, the peaks at 2θ values of 35.64°, 38.85°, and 48.75° were used. Meanwhile, for the CuO/Zn<sub>2</sub>SnO<sub>4</sub> composites, the peaks used were at 2θ values of 34.48°, 36.06°, and 38.85° for 20% CuO; 34.51°, 35.59°, and 38.93° for 40% CuO; 34.49°, 35.68°, and 38.90° for 60% CuO; and 34.45°, 35.67°, and 38.92° for 80% CuO. The calculated crystallite sizes are presented in Table 1.

From Table 1, it can be observed that the crystallite size of the composites is generally larger than that of pure Zn<sub>2</sub>SnO<sub>4</sub> and CuO, with a tendency to increase as the CuO content in the composite increases. This indicates that the addition of CuO influences the crystal formation of the CuO/Zn<sub>2</sub>SnO<sub>4</sub> composites. Although the differences in crystallite size among the six samples are not highly significant, crystallite size remains an important factor influencing the photocatalytic performance of the resulting composite [33]. Larger crystallite sizes can enhance the amount of absorbed energy, reduce the recombination rate of electron (e<sup>-</sup>) and hole (h<sup>+</sup>) pairs, and facilitate charge transfer to the surface of the composite. These factors collectively enhance the redox reactions occurring on the catalyst surface, promoting the conversion of H<sub>2</sub>O, OH<sup>-</sup>, and O<sub>2</sub> into free radicals, which are essential for the degradation of ciprofloxacin antibiotics and other organic pollutants [34].

### 3.2. SEM and TEM Analysis

The shape and morphology of the synthesized materials were analyzed using SEM and TEM, as presented in Figure 2. Based on the SEM analysis shown in Figure 2a, the morphology of Zn<sub>2</sub>SnO<sub>4</sub> is predominantly characterized by irregularly spherical particles, with a small portion exhibiting an octahedral shape. This observation was further confirmed by TEM analysis, which showed a particle size of approximately 68.33 nm, as illustrated in Figure 2b. In comparison, the morphology of the synthesized CuO nanoparticles observed through SEM (Figure 2c) revealed that the CuO nanoparticles possess a square sheet-like structure with an average size of 116.94 nm. This morphological feature was also supported by TEM analysis (Figure 2d), which confirmed the presence of well-defined sheet-like structures.

Further, SEM characterization was carried out on CuO/Zn<sub>2</sub>SnO<sub>4</sub> composites with varying CuO concentrations, as shown in Figure 3. In Figure 3a, for the composite containing 20% CuO, the morphology shows a combination of square sheets corresponding to Zn<sub>2</sub>SnO<sub>4</sub> and spherical or round sheets corresponding to CuO particles. As the concentration of CuO increases (Figures 3b-d), there is a significant increase in the number of sheet-like CuO particles, indicating good dispersion and successful integration of CuO into the composite structure. This trend is also consistent with the increasing diffraction intensity of CuO peaks observed in the XRD pattern (Figure 1b).

Furthermore, the morphology of the CuO/Zn<sub>2</sub>SnO<sub>4</sub> composite was confirmed by TEM analysis, as shown in Figure 3e. TEM results reveal that the nanoparticles of the CuO/Zn<sub>2</sub>SnO<sub>4</sub> composite are irregularly shaped square and round sheets with an average particle size of 69.53 nm at a CuO concentration of 40% w/w. Variations in morphology and particle size are key factors that influence the photocatalytic performance of the composite. Both factors are closely related to the increase in the active surface area, improved surface interactions with target molecules, and enhanced sensitivity of the resulting composite [31, 35].

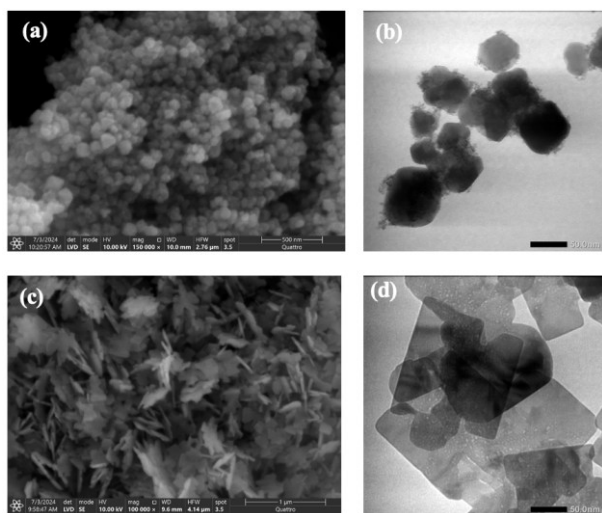


Figure 2. SEM images of (a)  $Zn_2SnO_4$  and (c)  $CuO$ ; TEM images of (b)  $Zn_2SnO_4$  and (d)  $CuO$

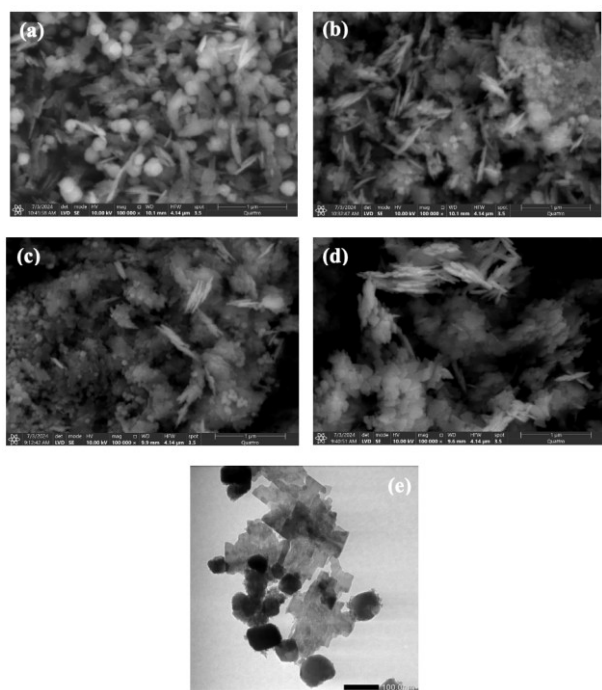


Figure 3. SEM micrographs of  $CuO/Zn_2SnO_4$  composites with varying  $CuO$  concentrations: (a) 20%, (b) 40%, (c) 60%, and (d) 80%, and (e) TEM micrograph of the composite with 40%  $CuO$  concentration

### 3.3. UV-Vis DRS Analysis

The optical properties of the synthesized materials were characterized using a UV-Vis DRS spectrophotometer. The band gap energy of each sample was determined by applying the Kubelka–Munk function. The reflectance analysis results obtained from the UV-Vis DRS measurements, along with the corresponding plots of  $(F(R)hv)^2$  versus photon energy (eV), are presented in Figure 4.

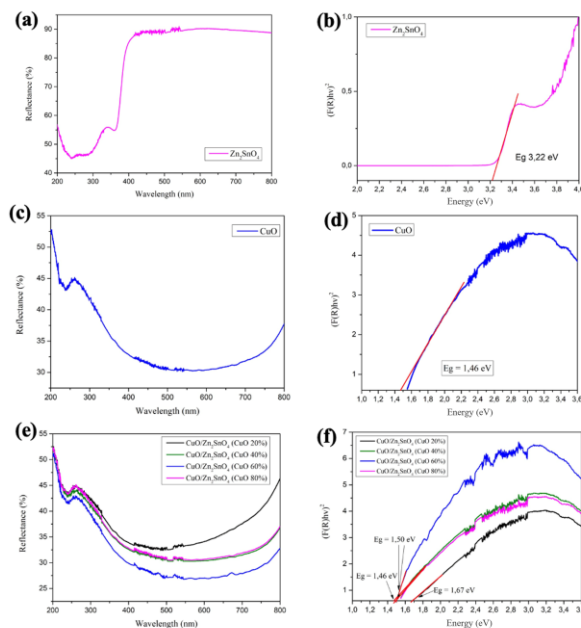


Figure 4. UV-Vis DRS spectra of the samples: (a) reflectance of  $Zn_2SnO_4$ , (b)  $(F(R)hv)^2$  vs. energy plot of  $Zn_2SnO_4$ , (c) reflectance of  $CuO$ , (d)  $(F(R)hv)^2$  vs. energy plot of  $CuO$ , (e) reflectance of  $CuO/Zn_2SnO_4$  composites with varying  $CuO$  concentrations, and (f)  $(F(R)hv)^2$  vs. energy plot of  $CuO/Zn_2SnO_4$  composites with varying  $CuO$  concentrations

The band gap values of  $Zn_2SnO_4$  and  $CuO$  before compositing were determined to be 3.22 eV and 1.46 eV, respectively, as shown in Figures 4a-d. After compositing with 20%  $CuO$ , the band gap of  $Zn_2SnO_4$  decreased to 1.67 eV. Increasing the  $CuO$  concentration to 40% reduced the band gap to 1.46 eV. At higher  $CuO$  concentrations of 60% and 80%, the band gap values remained relatively stable at around 1.50 eV (Figures 4e and 4f). This decrease in band gap is closely related to the higher  $CuO$  content [26, 36]. The reduction occurs due to enhanced charge transfer from the valence band to the conduction band of  $CuO$ , associated with the d–d transitions of  $Cu^{2+}$  ions. As a result, the material’s ability to absorb visible light improves, facilitating the formation of electron-hole pairs and enhancing the photocatalytic performance of the synthesized composites [27, 37, 38].

### 3.4. Photodegradation of the Antibiotic Ciprofloxacin

The photocatalytic performance of the synthesized materials was evaluated by testing their ability to degrade ciprofloxacin antibiotic solution under direct sunlight irradiation. The degradation process was monitored using a UV-Vis spectrophotometer, and the resulting spectra for the ciprofloxacin solution degraded by  $Zn_2SnO_4$ ,  $CuO$ , and the  $CuO/Zn_2SnO_4$  nanocomposite with 20%  $CuO$  at various irradiation times are presented in Figure 5.

**Table 2.** Surface area, porosity characteristics, and photodegradation efficiency of ciprofloxacin using various catalysts

Catalyst	Light intensity (watts/m <sup>2</sup> )	Surface area (m <sup>2</sup> /g)	Pore volume (cm <sup>3</sup> /g)	Pore size (Å)	Percentage of degradation (%)
Zn <sub>2</sub> SnO <sub>4</sub>	635.713	79.279	0.237	111.359	78.30
CuO	635.713	15.708	0.042	116.046	-8.87
CuO/Zn <sub>2</sub> SnO <sub>4</sub> nanocomposite (CuO 20%)	635.713	37.133	0.161	169.355	47.07

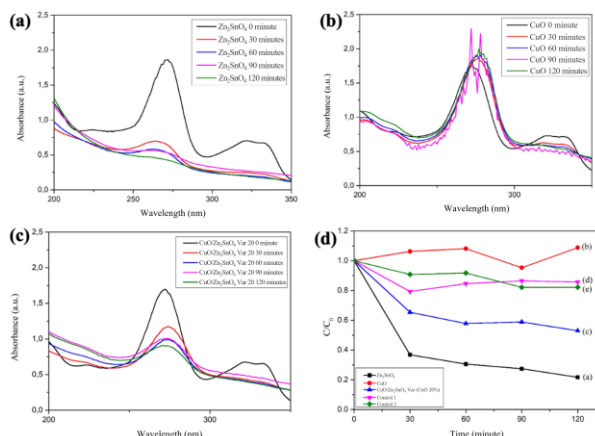


**Figure 5.** UV-Vis spectrophotometer spectra of ciprofloxacin solution after 120 minutes of irradiation with catalyst treatment: (a) Zn<sub>2</sub>SnO<sub>4</sub>, (b) CuO, (c) CuO/Zn<sub>2</sub>SnO<sub>4</sub> nanocomposite (CuO 20%), and (d) photodegradation rate of ciprofloxacin as a function of irradiation time for each catalyst treatment

From Figure 5, it can be observed that the ciprofloxacin absorbance peak decreases significantly when using Zn<sub>2</sub>SnO<sub>4</sub> (Figure 5a) and the CuO/Zn<sub>2</sub>SnO<sub>4</sub> nanocomposite (Figure 5c) with increasing irradiation time. This decrease in absorbance indicates the progressive degradation of the ciprofloxacin antibiotic by both catalysts, with degradation percentages of 78% and 47%, respectively, after 120 minutes of irradiation. In contrast, using CuO alone does not show a significant reduction in the ciprofloxacin absorption peak, confirming that CuO is ineffective as a standalone photocatalyst for ciprofloxacin degradation (Figure 5b).

Furthermore, Figure 5d illustrates the change in ciprofloxacin concentration over the irradiation time, where C<sub>0</sub> represents the initial concentration before irradiation, and C is the concentration at each time interval. It is evident from Figure 5d that the highest rate of ciprofloxacin degradation occurs with Zn<sub>2</sub>SnO<sub>4</sub> and the CuO/Zn<sub>2</sub>SnO<sub>4</sub> nanocomposite. Additionally, the low degradation rates observed in control sample 1 (catalyst without irradiation) and control sample 2 (irradiation without catalyst) confirm that the reduction in ciprofloxacin concentration is primarily due to the photocatalytic activity of Zn<sub>2</sub>SnO<sub>4</sub> and the CuO/Zn<sub>2</sub>SnO<sub>4</sub> nanocomposite.

Although CuO is known to be an effective co-catalyst [39], possessing a large penetration coefficient [23, 24], and capable of reducing the band gap of Zn<sub>2</sub>SnO<sub>4</sub> from 3.22 eV to 1.46 eV—thereby enhancing the light response in the visible region—the CuO/Zn<sub>2</sub>SnO<sub>4</sub> nanocomposite does not exhibit better photocatalytic performance compared

to pure Zn<sub>2</sub>SnO<sub>4</sub>. This phenomenon is believed to be closely related to the surface characteristics of the composite, specifically a reduction in surface area and pore volume, along with an increase in pore size with the addition of CuO, as measured using the Brunauer–Emmett–Teller (BET) method, as presented in Table 2. From Table 2, it can be observed that Zn<sub>2</sub>SnO<sub>4</sub> has a larger surface area and pore volume compared to both CuO and the CuO/Zn<sub>2</sub>SnO<sub>4</sub> nanocomposites. Consequently, the larger surface area of Zn<sub>2</sub>SnO<sub>4</sub> facilitates more effective adsorption of ciprofloxacin, H<sub>2</sub>O<sub>2</sub>, OH<sup>-</sup>, and O<sub>2</sub>, all of which are key factors in generating free radicals, thereby enhancing the photocatalytic performance of the catalyst [15, 40].

#### 4. Conclusion

Based on the results of this study, CuO/Zn<sub>2</sub>SnO<sub>4</sub> nanocomposites were successfully synthesized with varying CuO concentrations of 20%, 40%, 60%, and 80% (w/w). The morphology analysis showed that the CuO/Zn<sub>2</sub>SnO<sub>4</sub> nanocomposites exhibited square-sheet structures corresponding to CuO and irregular spherical shapes corresponding to Zn<sub>2</sub>SnO<sub>4</sub>, with an average particle size of 69.53 nm. The band gap values of the synthesized composites decreased from 3.22 eV for pure Zn<sub>2</sub>SnO<sub>4</sub> to 1.67 eV (20% CuO), 1.46 eV (40% CuO), and stabilized around 1.50 eV for higher CuO concentrations (60% and 80%). This indicates improved light absorption in the visible region. The photocatalytic performance test for ciprofloxacin degradation revealed degradation efficiencies of 78.30% for pure Zn<sub>2</sub>SnO<sub>4</sub>, -8.87% for pure CuO, and 47.07% for the CuO/Zn<sub>2</sub>SnO<sub>4</sub> nanocomposite with 20% CuO after 120 minutes of sunlight irradiation. Furthermore, the presence of CuO in the composite resulted in a reduction of surface area from 79.279 m<sup>2</sup>/g (Zn<sub>2</sub>SnO<sub>4</sub>) to 37.133 m<sup>2</sup>/g, a decrease in pore volume from 0.237 cm<sup>3</sup>/g to 0.161 cm<sup>3</sup>/g, and an increase in pore size from 111.359 Å to 169.355 Å. These changes contributed to a decline in photocatalytic performance. Overall, this study confirms that surface area is a critical factor influencing the photocatalytic efficiency of CuO/Zn<sub>2</sub>SnO<sub>4</sub> nanocomposites in degrading ciprofloxacin antibiotics.

#### Acknowledgments

The authors would like to thank the Ministry of Education, Culture, Research, and Technology for the financial support provided through the 2024 Master's Thesis Research Scheme (PTM) under contract number 3951/UN30.15/PT/2024.

## References

- [1] Dino Rimantho, Athiyah Athiyah, Analisis Kapabilitas Proses Untuk Pengendalian Kualitas Air Limbah Di Industri Farmasi, *Jurnal Teknologi*, 11, 1, (2019), 1-8
- [2] Klaudia Kulik, Anna Lenart-Boroń, Kinga Wyrzykowska, Impact of Antibiotic Pollution on the Bacterial Population within Surface Water with Special Focus on Mountain Rivers, *Water*, 15, 5, (2023), 975 <https://doi.org/10.3390/w15050975>
- [3] Xuan Zhu, Tsang Daniel C. W., Chen Feng, Li Shiyu, Xin and Yang, Ciprofloxacin adsorption on graphene and granular activated carbon: kinetics, isotherms, and effects of solution chemistry, *Environmental Technology*, 36, 24, (2015), 3094-3102 <https://doi.org/10.1080/09593330.2015.1054316>
- [4] Zhidong Wei, Junying Liu, Wenfeng Shangguan, A review on photocatalysis in antibiotic wastewater: Pollutant degradation and hydrogen production, *Chinese Journal of Catalysis*, 41, 10, (2020), 1440-1450 [https://doi.org/10.1016/S1872-2067\(19\)63448-0](https://doi.org/10.1016/S1872-2067(19)63448-0)
- [5] Daesub Hwang, Jun-Su Jin, Horim Lee, Hae-Jin Kim, Heejae Chung, Dong Young Kim, Sung-Yeon Jang, Dongho Kim, Hierarchically Structured Zn<sub>2</sub>SnO<sub>4</sub> Nanobeads for High-Efficiency Dye-Sensitized Solar Cells, *Scientific Reports*, 4, 1, (2014), 7353 <https://doi.org/10.1038/srep07353>
- [6] Francis Paquin, Jonathan Rivnay, Alberto Salleo, Natalie Stingelin, Carlos Silva-Acuña, Multi-phase microstructures drive exciton dissociation in neat semicrystalline polymeric semiconductors, *Journal of Materials Chemistry C*, 3, 41, (2015), 10715-10722 <https://doi.org/10.1039/C5TC02043C>
- [7] Oussama Baaloudj, Achraf Amir Assadi, Mohamed Azizi, Hamza Kenfoud, Mohamed Trari, Abdeltif Amrane, Aymen Amine Assadi, Nouredine Nasrallah, Synthesis and Characterization of ZnBi<sub>2</sub>O<sub>4</sub> Nanoparticles: Photocatalytic Performance for Antibiotic Removal under Different Light Sources, *Applied Sciences*, 11, 9, (2021), 3975 <https://doi.org/10.3390/app11093975>
- [8] Beibei Wang, Kejiang Qian, Weiping Yang, Wenjing An, Lan-Lan Lou, Shuangxi Liu, Kai Yu, ZnFe<sub>2</sub>O<sub>4</sub>/BiVO<sub>4</sub> Z-scheme heterojunction for efficient visible-light photocatalytic degradation of ciprofloxacin, *Frontiers of Chemical Science and Engineering*, 17, 11, (2023), 1728-1740 <https://doi.org/10.1007/s11705-023-2322-z>
- [9] Shahzaib Khan, Muhammad Usman, Muhammad Abdullah, Muhammad Suleman Waheed, Muhammad Faheem Ashiq, Muhammad Ishfaq Ahmad, Abdunnasser M. Karami, Muhammad Fahad Ehsan, Sumaira Manzoor, Muhammad Naem Ashiq, Facile synthesis of CuAl<sub>2</sub>O<sub>4</sub>/rGO nanocomposite via the hydrothermal method for supercapacitor applications, *Fuel*, 357, (2024), 129688 <https://doi.org/10.1016/j.fuel.2023.129688>
- [10] Kyung-Won Jeon, Ji-Woo Park, Ru-Ri Lee, Ji-Hyeon Gong, Won-Jun Jang, Jae-Oh Shim, Young-Wan Ju, Facile synthesis of CuFe<sub>2</sub>O<sub>4</sub> catalyst by the electrospinning method to produce hydrogen via the water gas shift of waste-derived syngas, *Journal of Environmental Chemical Engineering*, 11, 3, (2023), 110105 <https://doi.org/10.1016/j.jece.2023.110105>
- [11] Hong Fan, Shucong Xu, Xianmin Cao, Daoxi Liu, Yaoyu Yin, Haiyong Hao, Dezhou Wei, Yanbai Shen, Ultra-long Zn<sub>2</sub>SnO<sub>4</sub>-ZnO microwires based gas sensor for hydrogen detection, *Applied Surface Science*, 400, (2017), 440-445 <https://doi.org/10.1016/j.apsusc.2016.12.221>
- [12] Xiaofei Hu, Hongshun Hao, Weihua Guo, Shanshan Jin, Hong Li, Hongman Hou, Gongliang Zhang, Shuang Yan, Wenyuan Gao, Guishan Liu, Hydrothermal synthesis, characterization and enhanced visible-light photocatalytic activity of Co-doped Zn<sub>2</sub>SnO<sub>4</sub> nanoparticles, *Chemical Physics*, 490, (2017), 38-46 <https://doi.org/10.1016/j.chemphys.2017.04.001>
- [13] Jie Lu, Yanmei Xie, Fuli Luo, Hao Fu, Xiang Huang, Yuchang Liu, Hongjie Liu, Heterostructures of mesoporous hollow Zn<sub>2</sub>SnO<sub>4</sub>/SnO<sub>2</sub> microboxes for high-performance acetone sensors, *Journal of Alloys and Compounds*, 844, (2020), 155788 <https://doi.org/10.1016/j.jallcom.2020.155788>
- [14] Ana Rovisco, Rita Branquinho, Jonas Deuermeier, Tomás Freire, Elvira Fortunato, Rodrigo Martins, Pedro Barquinha, Shape Effect of Zinc-Tin Oxide Nanostructures on Photodegradation of Methylene Blue and Rhodamine B under UV and Visible Light, *ACS Applied Nano Materials*, 4, 2, (2021), 1149-1161 <https://doi.org/10.1021/acsanm.0c02782>
- [15] Eka Angasa, Asdim, Zulhadjri, Novesar Jamarun, Syukri Arief, The effect of *Impatiens balsamina* L. extract on structural, morphological, optical, and photocatalytic properties of Zn<sub>2</sub>SnO<sub>4</sub>, *Journal of Materials Research and Technology*, 9, 6, (2020), 12917-12925 <https://doi.org/10.1016/j.jmrt.2020.09.017>
- [16] Ana Rovisco, Maria Morais, Rita Branquinho, Elvira Fortunato, Rodrigo Martins, Pedro Barquinha, Microwave-Assisted Synthesis of Zn<sub>2</sub>SnO<sub>4</sub> Nanostructures for Photodegradation of Rhodamine B under UV and Sunlight, *Nanomaterials*, 12, 12, (2022), 2119 <https://doi.org/10.3390/nano12122119>
- [17] Qian Zhang, Youmei Li, Junbo Zhong, Jianzhang Li, Facile construction of CuO/g-C<sub>3</sub>N<sub>4</sub> heterojunctions with promoted photocatalytic hydrogen generation behaviors, *Fuel*, 353, (2023), 129224 <https://doi.org/10.1016/j.fuel.2023.129224>
- [18] Eka Angasa, Yulia Eka Putri, Zulhadjri, Novesar Jamarun, Syukri Arief, Improving the morphological, optical, and photocatalytic properties of octahedral Zn<sub>2</sub>SnO<sub>4</sub> using *Garcinia mangostana* fruit peel extract, *Vacuum*, 182, (2020), 109719 <https://doi.org/10.1016/j.vacuum.2020.109719>
- [19] Tayyebeh Soltani, Ahmad Tayyebi, Byeong-Kyu Lee, Photocatalysis and photocatalysis of tetracycline by sonochemically heterojunctioned BiVO<sub>4</sub>/reduced graphene oxide under visible-light irradiation, *Journal of Environmental Management*, 232, (2019), 713-721 <https://doi.org/10.1016/j.jenvman.2018.11.133>
- [20] Tiekun Jia, Ming Liu, Dongsheng Yu, Fei Long, Shuyi Mo, Zhao Deng, Weimin Wang, A Facile Approach for the Synthesis of Zn<sub>2</sub>SnO<sub>4</sub>/BiOBr Hybrid Nanocomposites with Improved Visible-Light Photocatalytic Performance, *Nanomaterials*, 8, 5, (2018), 313 <https://doi.org/10.3390/nano8050313>

- [21] V. Ramasamy Raja, D. Rani Rosaline, A. Suganthi, M. Rajarajan, Facile sonochemical synthesis of  $Zn_2SnO_4-V_2O_5$  nanocomposite as an effective photocatalyst for degradation of Eosin Yellow, *Ultrasonics Sonochemistry*, 44, (2018), 310-318 <https://doi.org/10.1016/j.ultsonch.2018.02.043>
- [22] Kai Huang, Tingting Hu, Yang Wang, Enhanced photocatalytic degradation of methylene blue through synthesizing of novel of  $BiVO_4/Zn_2SnO_4$  under visible light, *Journal of Solid State Chemistry*, 294, (2021), 121864 <https://doi.org/10.1016/j.jssc.2020.121864>
- [23] A. Zare, A. Saadati, S. Sheibani, Modification of a Z-scheme  $ZnO-CuO$  nanocomposite by Ag loading as a highly efficient visible light photocatalyst, *Materials Research Bulletin*, 158, (2023), 112048 <https://doi.org/10.1016/j.materresbull.2022.112048>
- [24] Yendrapati Taraka Prabhu, V. Navakoteswara Rao, Muthukonda Venkatakrishnan Shankar, Bojja Sreedhar, Ujjwal Pal, The facile hydrothermal synthesis of  $CuO@ZnO$  heterojunction nanostructures for enhanced photocatalytic hydrogen evolution, *New Journal of Chemistry*, 43, 17, (2019), 6794-6805 <https://doi.org/10.1039/c8nj06056h>
- [25] M. Chandrasekar, M. Subash, S. Logambal, G. Udhayakumar, R. Uthrakumar, C. Inmozhi, Wedad A. Al-Onazi, Amal M. Al-Mohaimed, Tse-Wei Chen, K. Kanimozhi, Synthesis and characterization studies of pure and Ni doped  $CuO$  nanoparticles by hydrothermal method, *Journal of King Saud University - Science*, 34, 3, (2022), 101831 <https://doi.org/10.1016/j.jksus.2022.101831>
- [26] M. Seethalakshmi, M. Shanthi, S. Dhanapandian, K. Ashokkumar, Hydrothermally synthesized various morphological  $CuO$  nanoparticles for stable and enhanced supercapacitor applications, *Research Square*, (2024), <https://doi.org/10.21203/rs.3.rs-3979204/v1>
- [27] Aadil Ahmad Bhat, Insaaf Assadullah, Aaliyah Farooq, Khurshaid Ahmad Malik, Javied Hamid Malik, Radha Tomar, Ishtihadah Islam, Atif Mossad Ali, Shakeel Ahmad Khandy, Band-gap alteration of  $Zn_2SnO_4$  nanostructures for optical and photoluminescent applications, *Materials Chemistry and Physics*, 306, (2023), 127993 <https://doi.org/10.1016/j.matchemphys.2023.127993>
- [28] Yan Yu, Binghua Yao, Baoyue Cao, Wei Ma, Morphology-controlled Fabrication of  $SnO_2/ZnO$  Nanocomposites with Enhanced Photocatalytic Performance, *Photochemistry and Photobiology*, 95, 5, (2019), 1131-1141 <https://doi.org/10.1111/php.13101>
- [29] Pietro Morozzi, Barbara Ballarin, Sara Arcozzi, Erika Brattich, Franco Lucarelli, Silvia Nava, Pedro José Gómez-Cascales, J. A. G. Orza, Laura Tositti, Ultraviolet-Visible Diffuse Reflectance Spectroscopy (UV-Vis DRS), a rapid and non-destructive analytical tool for the identification of Saharan dust events in particulate matter filters, *Atmospheric Environment*, 252, (2021), 118297 <https://doi.org/10.1016/j.atmosenv.2021.118297>
- [30] Ngia Masta, *Buku Materi Pembelajaran Scanning Electron Microscopy*, Universitas Kristen Indonesia, Jakarta, 2020,
- [31] D. M. Ibrahim, R. M. Mahani, M. N. Shaaban, M. El Maghraby, N. Mahmoud, A. A. Gaber, Synthesis of zinc stannate compounds utilizing natural cassiterite mineral, *Ceramics International*, 51, 6, (2025), 7728-7741 <https://doi.org/10.1016/j.ceramint.2024.12.211>
- [32] Gregor Žerjav, Albin Pintar, Influence of  $TiO_2$  Morphology and Crystallinity on Visible-Light Photocatalytic Activity of  $TiO_2-Bi_2O_3$  Composite in AOPs, *Catalysts*, 10, 4, (2020), 395 <https://doi.org/10.3390/catal10040395>
- [33] Abdullah Al Mamun Sakib, Shah Md. Masum, Jan Hoinkis, Rafiqul Islam, Md. Ashraf Islam Molla, Synthesis of  $CuO/ZnO$  Nanocomposites and Their Application in Photodegradation of Toxic Textile Dye, *Journal of Composites Science*, 3, 3, (2019), 91 <https://doi.org/10.3390/jcs3030091>
- [34] Asep Bayu Dani Nandiyanto, Rena Zaen, Rosi Oktiani, Correlation between crystallite size and photocatalytic performance of micrometer-sized monoclinic  $WO_3$  particles, *Arabian Journal of Chemistry*, 13, 1, (2020), 1283-1296 <https://doi.org/10.1016/j.arabjc.2017.10.010>
- [35] I. Sugihartono, I. Isnaeni, R. S. Mohar, W. Widiasih, The Effects of Growth Time on Surface Morphology and Optical Band Gap Energy  $ZnO$  Thin Films, *Journal of Physics: Conference Series*, 2377, (2022), 012011 <https://doi.org/10.1088/1742-6596/2377/1/012011>
- [36] Siti Barokah, Nuni Widiarti, Aktivitas Fotokatalitik  $CuO/ZnO$  pada Reaksi Oksidasi Fenol, *Indonesian Journal of Chemical Science*, 4, 2, (2015), 89-93
- [37] Ching-Tai Fu, Chia-Tung Kuo, Chong-Chi Chi, Lu-Cheng Hou, Chao- I. Liu, Shu-Chih Chang, Yuan-Mau Lee, Yu-Hsuan Chuang, Tri-Rung Yew, Photoactive Copper-Doped Zinc Stannate Thin Films for Ultraviolet-Visible Light Photodetector, *Journal of Electronic Materials*, 51, 9, (2022), 4884-4895 <https://doi.org/10.1007/s11664-022-09709-1>
- [38] Quanquan Shi, Guicheng Ping, Xiaojia Wang, Hui Xu, Jingmei Li, Jiaqi Cui, Hadi Abroshan, Hongjing Ding, Gao Li,  $CuO/TiO_2$  heterojunction composites: an efficient photocatalyst for selective oxidation of methanol to methyl formate, *Journal of Materials Chemistry A*, 7, 5, (2019), 2253-2260 <https://doi.org/10.1039/c8ta09439j>
- [39] Jian Yuan, Mingxia Chen, Jianwei Shi, Wenfeng Shangguan, Preparations and photocatalytic hydrogen evolution of N-doped  $TiO_2$  from urea and titanium tetrachloride, *International Journal of Hydrogen Energy*, 31, 10, (2006), 1326-1331 <https://doi.org/10.1016/j.ijhydene.2005.11.016>
- [40] Qinqin Zhao, Xiaolong Deng, Meng Ding, Jinzhao Huang, Dianxing Ju, Xijin Xu, Synthesis of hollow cubic  $Zn_2SnO_4$  sub-microstructures with enhanced photocatalytic performance, *Journal of Alloys and Compounds*, 671, (2016), 328-333 <https://doi.org/10.1016/j.jallcom.2016.01.264>